ACS OMEGA

http://pubs.acs.org/journal/acsodf

Article

All-Atom Molecular Dynamics Simulations of Polyethylene Glycol (PEG) and LIMP-2 Reveal That PEG Penetrates Deep into the Proposed CD36 Cholesterol-Transport Tunnel

Paul Dalhaimer* and Kate R. Blankenship

Cite This: *ACS Omega* 2022, 7, 15728−15738

Read Online

ACCESS | Metrics & More | Article Recommendations | Supporting Information

ABSTRACT: Polyethylene glycol (PEG) is the most prominent clinically administered synthetic polymer. For example, over 300 million people have been administered PEGylated liposome vaccines for SARS-CoV-2. PEG is used in mammals because it has low affinity for most proteins and vice versa. However, this makes it difficult to study the few interactions with proteins that PEG has. On the atomistic level, there are two PEG-protein structures: (1) PEG-LIMP-2 and (2) PEG-αPEG. In the first structure, two monomers of a 1.5 kDa PEG polymer (PEG2) had electron density deep in the postulated cholesterol transport tunnel of LIMP-2, a lysosomal cholesterol transport protein and member of the CD36 super family of proteins. It is unclear how PEG entered this tunnel. In the second structure, PEG wrapped around a surface-exposed tryptophan on its antibody. Since tryptophan is a rare residue, it is unclear if this PEG-Trp interaction is ubiquitous. To gain deeper mechanistic insight into PEG−protein interactions, we surrounded the LIMP-2 apo structure with 13 PEG chains of 10 monomers each (PEG10), water, and KCl and simulated the system using NAMD. One of the 13 chains penetrated LIMP-2 and came within 3 Å of PEG2. This was possible because of the strong hydrogen bonding between multiple oxygens along PEG10 and Arg192 but, most importantly, the clamping of the tertiary structure on PEG10. Clamping stabilized the movements of PEG10, and the leading oxygen of PEG10 was able to penetrate LIMP-2 and head toward to the position occupied by PEG2. Phe383 appears to act as a gate for objects to move through this cavity, which continues to the basal/membrane side of LIMP-2. Of all residues, PEG10 molecules had the most sustained interactions with lysine and arginine because of their strong hydrogen-bonding capabilities. These results show that the oxygens of PEG bind residues with high hydrogen bonding capabilities. However, the PEG−protein interaction is likely to be transient unless groups of resides can clamp down on PEG or a cavity that at least part of the PEG chain can enter is in close proximity to lower PEG's entropy.

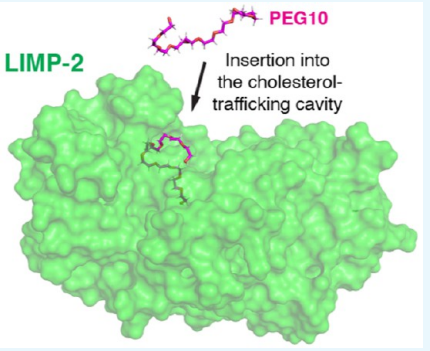

1. INTRODUCTION

Polyethylene glycol (PEG) is the most widely studied synthetic polymer in nanomedicine.[1] Its −C−C−O− repeating motif is hydrophilic, making it ideal for aqueous applications. It has low toxicity in mammals.[2] It is covalently conjugated to the exteriors of lipids that form the structural component of nanoparticles that are used for cancer chemotherapy (DOXIL) and vaccination in the clinic. These nanoparticles include the Pfizer and Moderna vaccines, where PEG is covalently linked to a subset of the lipid head groups that comprise the nanoparticle. PEG helps reduce protein accumulation on the exterior of these nanoparticles.[3] However, since it has such low affinity for most proteins, little is known about how it interacts with proteins. In fact, it is difficult to even approach the subject of PEG−protein interactions because the field does not have a solid starting point.

Very surprisingly, two monomers of PEG-1500 (1500 g/mol) had electron density in the crystal structure of lysosome membrane protein 2 (LIMP-2), a member of the CD36 super family of scavenger receptor proteins, which has a 34% identity and a 56% similarity to the major high-density lipoprotein (HDL) receptor, scavenger receptor class B I (SR-BI).[4] PEG binds SR-BI.[5] Thus, the CD36 family of proteins is especially important for PEG nanomedical applications because it is a potential entry point of PEG and PEG nanoparticles into cells. A crystal structure of SR-BI does not exist; however, given the presence of part of PEG-1500 in LIMP-2 and the high homology between LIMP-2 and SR-BI, we used LIMP-2 as a model CD36 family member to understand PEG−CD36 family interactions.

PEG was not known to interact with LIMP-2 a priori; it was used in the crystallization buffer to promote LIMP-2 packing.[4] In fact, PEG is widely used in crystallization buffers because it

Received: February 1, 2022
Accepted: April 18, 2022
Published: April 27, 2022

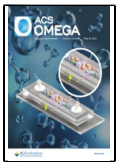

https://doi.org/10.1021/acsomega.2c00667
ACS Omega 2022, 7, 15728−15738

has high entropy, which increases depletion forces. Also, as mentioned above, PEG does not usually bind the protein that is being crystallized. In the LIMP-2 structure, Pro270, Thr365, and Lys381 were within 4.5, 3.6, and 2.5 Å of the two monomers of PEG-1500 in the tunnel that is postulated to be responsible for cholesterol transport in the CD36 superfamily.[4] Yet a hydrogen bond with Lys381 was the sole connecting feature between the two monomers of PEG-1500 and LIMP-2.[4] Thus, it is unclear how PEG-1500 was able to enter such a deep pocket in LIMP-2. The LIMP-2 crystals formed over 1−2 months, giving the PEG-1500 molecules uncountable opportunities to explore a vast conformational space. Given the lack of electron density for the other 30+ monomers of PEG-1500, it stands to reason that they were mobile.

The region of SR-BI that PEG binds is unknown.[5] Indeed, the middle monomers of PEG wrapped around its antibody at Trp96.[6] Thus, segments of PEG may interact with specific protein structural motifs that are yet to be determined. An approach that uses smaller, but still flexible, PEG molecules to explore the potential binding areas on the surface of the CD36 family of proteins may provide insight into the mechanisms by which PEG binds proteins. Thus, instead of using one PEG-1500 molecule in our simulations, we used PEG that had 10 monomers (PEG10) to explore as many of the PEG−LIMP-2 surface interactions as possible given computational time limitations.

We simulated Ile37-Ile429 of the endolysosome domain of the LIMP-2 crystal structure (PDB: 4F7B; DOI: 10.2210/pdb4F7B/pdb) with PEG having two monomers (PEG2) in its cholesterol binding pocket in a box of water and KCl for 60 ns. PEG2 was highly dynamic, interacted weakly with the surrounding residues, and formed hydrogen bonds mostly with the oxygen on the LIMP-2 backbone at Gly253. We removed PEG2 from the LIMP-2 crystal structure and surrounded the protein with 13 PEG molecules that each had 10 monomers (PEG10), water, and KCl. We simulated this system for 110 ns. We refer to this simulation as PEG10A. One of the 13 PEG10A molecules called HETI in the LIMP2-PEG10A.pdb file interacted strongly with Arg192. This allowed PEG10A/HETI to enter the notch flanked by α11 and the disordered region Pro193-Gly211. This is the opening of the proposed cholesterol transport tunnel in the CD36 super family of proteins.[4] Over ∼100 ns, the PEG10A/HETI molecule traveled from the exterior of the water box and inserted into this tunnel cavity in which it traveled within 3 Å of the position of PEG2 at the end of its own simulation when the structures were overlaid. One of the other PEG10A molecules called HETC interacted with Lys39, Lys419, and Lys426. PEG10A/HETC wrapped around Lys426 in a geometric configuration that was similar to the one assumed by PEG when it interacted with Trp96 of the PEG antibody.[6] In a separate simulation, which we call PEG10B, PEG10B/HETL penetrated the basal opening of the cholesterol transport tunnel at the membrane side of LIMP-2. PEG10 interacted strongly with lysines and arginines because of their numerous hydrogen-bonding capabilities. The simulations show that PEG can bind and enter protein cavities over short time scales if surface exposed lysines and arginines are available for hydrogen binding and PEG stabilization. However, the surface topology plays the major role in PEG10−LIMP-2 bonding persistence. PEG10 stayed bound to LIMP-2 only when groups of residues clamped down on regions of the PEG10. Our simulations uncover mechanisms for PEG−protein binding and have ramifications for the pharmacokinetics, pharmacodynamics, and toxicity of PEG-based nanomedicines.

2. SIMULATION METHODS

We used the CHARMM-GUI Glycan Reader & Modeler platform to set up the structure files for NAMD simulation.[7−12] Starting from chain A of the 4F7B.pdb structure file (DOI: 10.2210/pdb4F7B/pdb), we preserved the three *N*-acetyl-D-galactosamine glycosylation states at Asn45, Asn224, and Asn304.[4] The two disulfide bonds between C274−C329 and C312−C318 were preserved. All histidine residues were singly protonated at Nε. A salt concentration of 150 mM KCl, the approximate K^+ concentration in the mammalian cell,[13] was added to the water box via Monte Carlo. The PEG2 in the crystal structure was preserved for the LIMP-2−PEG2 simulations. The 10-mer PEG10 chains were built by the CHARMM-GUI polymer builder.[14] All coordinate (.pdb) files are available in the Supporting Information. We chose 10 monomers for a PEG length so that the polymer would be flexible enough to coil upon itself as would longer PEG molecules like PEG-1500 but short enough so that we could use multiple PEGs that could independently probe different binding locations on the surface of LIMP-2. PEG has a persistence length of ∼4 Å. Our PEG10 molecules have a contour length of ∼120 Å. All systems were equilibrated at 100, 200, and 300 K for 10 000 steps each. Each step consists of a global minimization of energy and has no link to a physical time. The total energy of the system changed by less than 10^{-5} kcal/mol from the second last step to the last step of each run. Production simulations were run at 310 K (37 °C) using NAMD2.14.[15] We used a constant-NPT ensemble with standard NAMD simulation parameters. The cutoff distance was 12.0 Å, the switchdist variable was 10.0 Å, and the pairlistdist variable was 16.0 Å. Particle mesh Ewald was used. Langevin dynamics were used to control the temperature and pressure. Simulation results were analyzed in VMD.[16] All images and movies of the simulations were generated using PyMol and VMD, respectively. The RMSD was calculated using the RMSD Trajectory tool in VMD. The Microsoft Excel autocorrelation function ACF(RMSD,time_step) in the Xreadstats-Mac add-in was used to calculate the autocorrelation of RMSD as a function of time.

3. RESULTS AND DISCUSSION

We used chain A of PDB: 4F7B (DOI: 10.2210/pdb4F7B/pdb) as our starting model (hereafter, LIMP-2). This region of LIMP-2 is in the lumen of late endosomes and lysosomes.[17] We modeled LIMP-2 from Ile37−Ile429.[2,18] We performed three major simulations: LIMP-2−apo (60 ns), LIMP-2−PEG2 (60 ns), LIMP-2−PEG10 (PEG10A) (110 ns), and LIMP-2−PEG10 (PEG10B) (75 ns). We used the CHARMM-GUI Web site to build and equilibrate our LIMP-2−apo, LIMP-2−PEG2, and LIMP-2−PEG10 models.[7,9,19] PyMol determined that LIMP-2 has 13 α-helices and 17 β-sheets (Figure 1A). Specific details on the structure can be found in ref 4. The proposed cholesterol transport tunnel is flanked by Pro270, Val277, Met337, Phe339, Ile376, Ala379, Lys381, and Val415 (Figure 1B).[18] PEG2 in the LIMP-2 crystal structure is located deep in the cholesterol tunnel near residues Pro270, Thr365, and Lys381 (Figure 1B).[4]

https://doi.org/10.1021/acsomega.2c00667
ACS Omega 2022, 7, 15728−15738

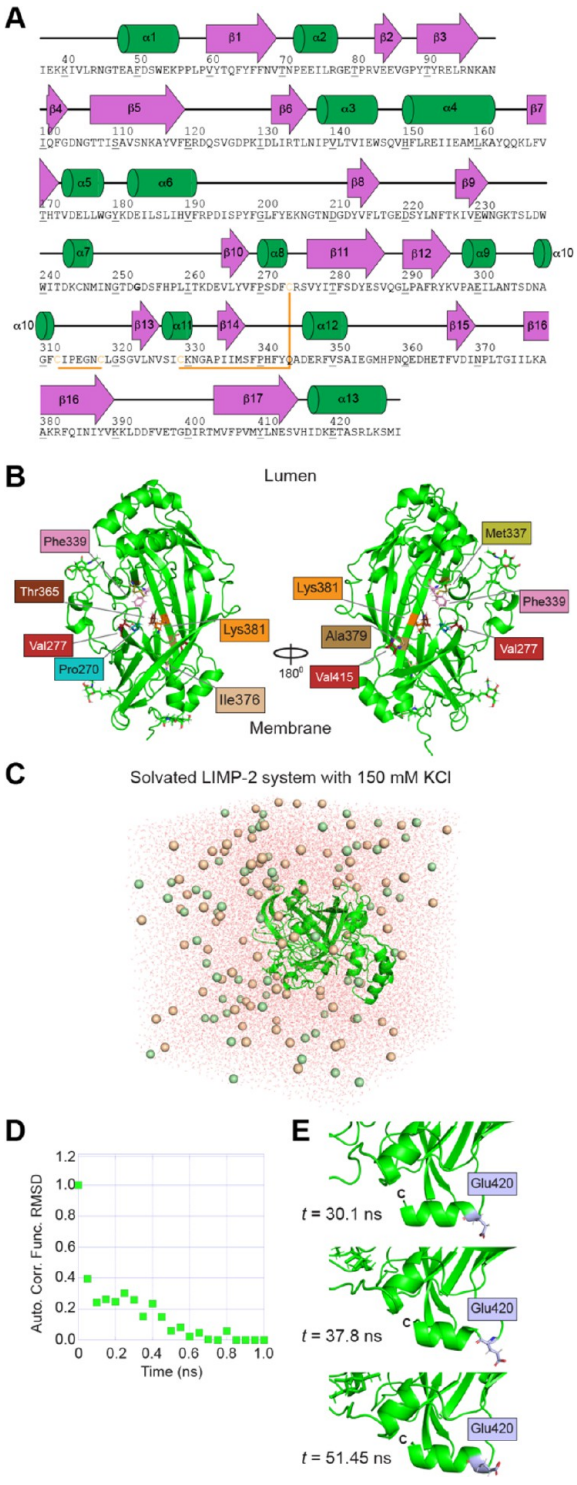

Figure 1. Structure, sequence, and simulation LIMP-2 apo. (A) Sequence and secondary structure of LIMP-2. Note the two disulfide bonds. (B) Ribbon diagrams of PDB: 4F7B. Residues that have been postulated to be important for PEG binding and cholesterol transport through LIMP-2 are highlighted. The lumen represents the interior of an endolysosome, and the membrane represents the membrane of an endolysosome. (C) Image of the simulation set up for the LIMP-2 apo simulation. The LIMP-2 crystal structure was surrounded with 10 Å padding of water in 150 mM KCl. Potassium ions are tan. Chloride ions are light green. (D) Plot of the autocorrelation of the root mean squared displacement (RMSD) of the backbone of LIMP-2 shown in (C). (E) Ribbon diagrams of the C-terminal region of LIMP-2 at the indicated simulation time points.

We took out the PEG2 from the LIMP-2 crystal structure (apo) and added water with a 10 Å padding around LIMP-2 and 150 mM KCl (Figure 1C). The system had 6363 protein atoms including glycosylated asparagine, 24 487 TIP3 water molecules, 87 potassium ions, and 69 calcium ions. We ran this system for 60 ns. The autocorrelation of the RMSD went to zero after ∼0.6 ns as measured by Microsoft Excel's ACF() function (Figure 1D; Movie S1). This indicates that the movements of LIMP-2 are uncorrelated from the equilibrated conformation after ∼0.6 ns. The secondary structure of LIMP-2 apo is stable over the 60 ns of simulation (Movie S1). The only area that shows secondary structure rearrangement is the α-helix from Glu420 to Ile429. It begins as an α-fold but unwinds slightly at the Glu420 end around $t \sim 37$ ns (Figure 1E). The helix refolds around $t \sim 50$ ns. This instability may be caused by the truncation of the LIMP-2 Leu433-Trp455 transmembrane domain.[4]

We studied the dynamics of the two-monomer PEG (PEG2) that was discovered in the crystal structure of LIMP-2.[4] PEG2 was located in the cholesterol transport tunnel region close to Gly253, Lys330, Thr365, Arg382, and Glu413 (Figure 2A). A surface representation of LIMP-2 shows PEG2 buried in the protein (Figure 2B). As stated, it is remarkable that PEG-1500 could deeply penetrate a protein.[4] This is the only protein structure we are aware of that has PEG electron density deep in the protein interior. The value of the autocorrelation function of the RMSD displacement of LIMP-2 decayed to zero at ∼0.6 ns (Figure 2C). This value is similar to the autocorrelation time of the LIMP-2 apo simulation. Over 60 ns of simulation time, PEG2 rarely formed more than one hydrogen bond with the surrounding residues and was highly dynamic (Figure 2D; Movie S2). Of these few interactions, PEG2 had the most frequent hydrogen-bond connections with Gly253, Thr365, Arg382, and Lys381 (Figure 2E). Of these residues, Thr365 and Lys381 were postulated to interact with PEG-1500 in the static crystal structure by proximity.[4] Here, we see the strongest interaction with the LIMP-2 backbone at Gly253. To quantify the movement of PEG2 in the cholesterol tunnel, we measured the distance between the first oxygen of PEG2 (O1) and the α-carbon of Gly253 (CA). There was an upward trend in the distance between these two atoms over the 60 ns of simulation time (Figure 2F). We examined the interactions of PEG2 with the surrounding molecules at the 10 time points where PEG2 had more than one hydrogen bond with surrounding residues as indicated by the rectangle in Figure 2D (Figure 2G−P). Many water molecules are present in this region of LIMP-2 and PEG2 makes at least one hydrogen bond with a water molecule at each of the time points except at $t = 33.4$ ns. PEG2 was stabilized by hydrogen bonds to LIMP-2 residues at its O1 and O3 atoms in the situations where PEG2 had more than one hydrogen bond to LIMP-2 (Figure 2G−I,K−P). From $t = 0$ to ∼50 ns, PEG2 diffused in a well-defined area, but at $t \sim 52$ ns, PEG2 moved 6.8 Å toward the cholesterol cavity opening (Figure 2Q; Movie S2). At this new location, PEG2 had no hydrogen bonds with LIMP-2 (Figure 2R). The Phe383 ring moved/rotated 6.3 Å between $t = 52.0$ ns and $t = 52.7$ ns to allow PEG2 to diffuse underneath it and toward the LIMP-2 surface (Figure 2R; Movie S2). We did not observe PEG2 diffusing in the other direction, toward the LIMP-2 membrane domain, which has an opening that is the postulated transfer point of cholesterol to and from the endosome.

https://doi.org/10.1021/acsomega.2c00667
ACS Omega 2022, 7, 15728−15738

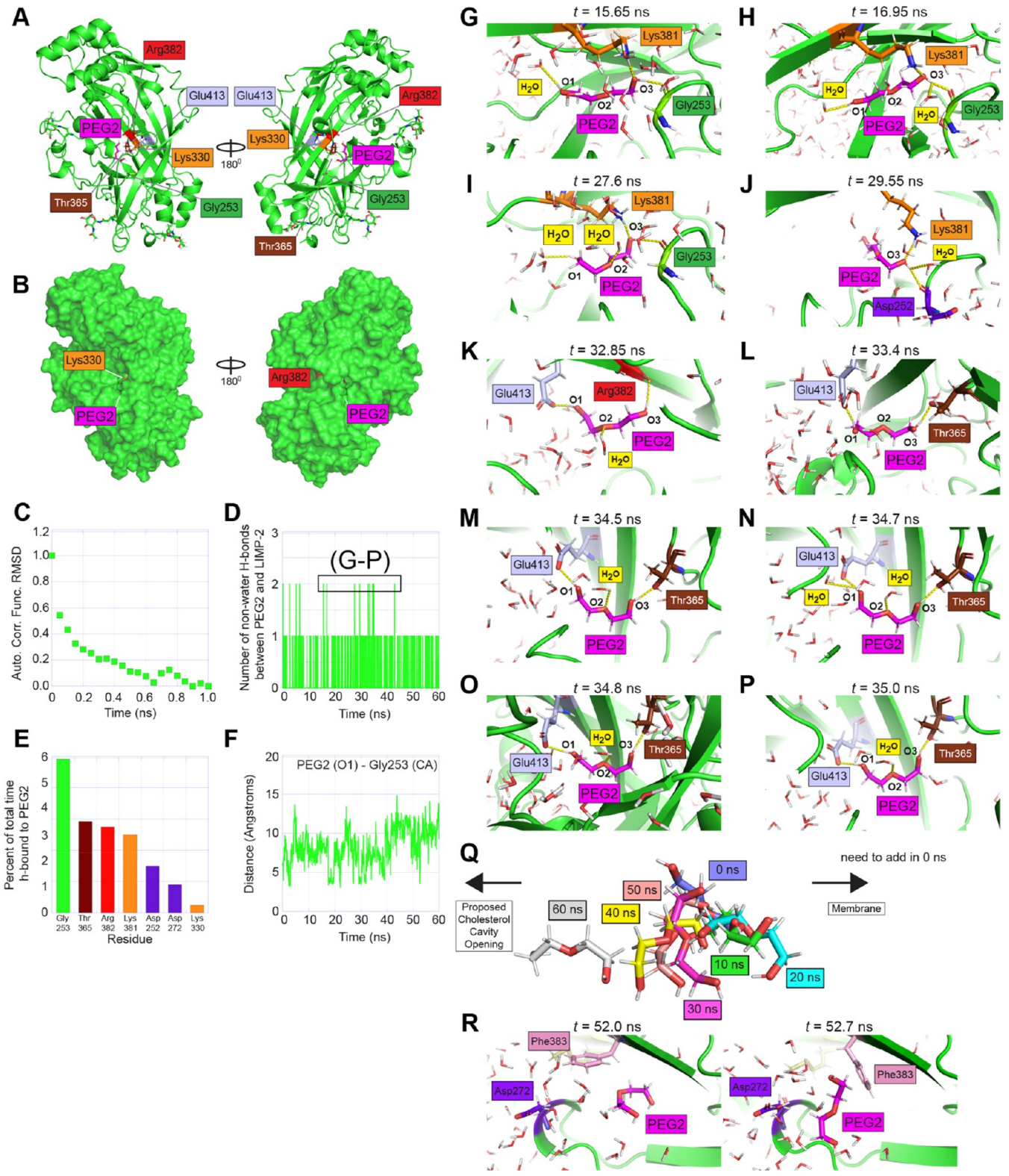

Figure 2. Dynamics of the PEG molecule (PEG2) found in the crystal structure of LIMP-2 from ref 4. (A) Ribbon diagram of LIMP-2 with PEG2 (magenta) and surrounding residues highlighted. (B) Space-filled model of LIMP-2 with PEG2 (magenta) and Lys330 highlighted. (C) Plot of the autocorrelation of the RMSD of the backbone of LIMP-2 (D) Plot of the number of hydrogen bonds of PEG2 with neighboring residues over the time course of the simulation. Hydrogen bonds with water molecules were not included in this plot. (E) Plot of the percent time that PEG2 was hydrogen-bonded to the indicated residues over the course of the simulation. (F) Plot of the distance between the first oxygen of PEG2 (O1) and the α-carbon of Gly253 (CA) over the time course of the simulation. (G−P) Diagrams of the interactions of PEG2 with neighboring residues at the time points when the number of hydrogen bonds was highest as indicated in (D). (Q) Overlay of PEG2 at the indicated time points. (R) Diagrams of the interactions of PEG2 with Asp272 and Ph383 before and after PEG2 moved a significant distance as shown in (Q).

https://doi.org/10.1021/acsomega.2c00667
ACS Omega 2022, 7, 15728−15738

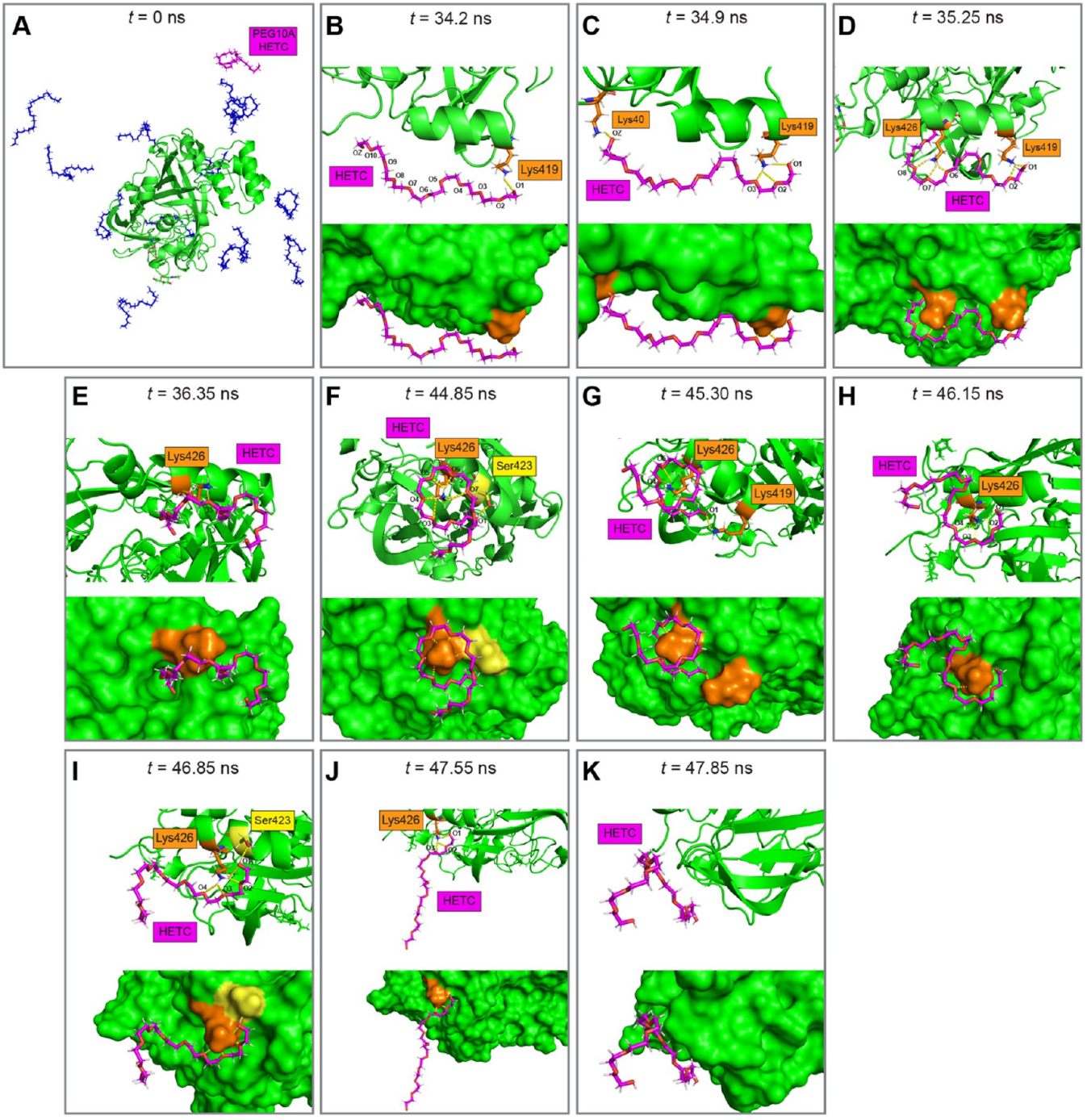

Figure 3. PEG10A/HETC wraps around surface exposed lysine residues. (A) Starting configuration of the simulation where LIMP-2 was surrounded by 13 randomly positioned PEG molecules having 10 monomers each (PEG10). PEG10A/HETC (magenta) is the focus of this figure. Water and KCl were removed in this image. (B–K) Ribbon diagrams and matching space-filled images of PEG10A/HETC interacting with LIMP-2 residues at the indicated time points.

To determine the mechanisms by which PEG interacts with LIMP-2 from an unbiased starting point, we randomly surrounded LIMP-2 with 13 PEG molecules that had 10-monomers each (PEG10) (Figure 3A). We simulated this system for 110 ns (Movie S3). This simulation is called PEG10A and the 13 PEG10 molecules in it are referred to as PEG10A/HET#, where # represents the letter of that heteroatom in the Supporting Information PDB file (LIMP2-PEG10A.pdb). O1 of the PEG10A/HETC molecule made a hydrogen bond with Lys419 at t = 34.2 ns, which persisted until 34.35 ns (Figure 3B; Movie S4). At t = 34.9 ns, O1–O3 form three hydrogen bonds with Lys419 and OZ forms a hydrogen bond with Lys40 (Figure 3C). PEG10A/HETC stretched to an end-to-end length of 23.1 Å in this conformation. The middle section of PEG10A/HETC was within 5 Å of Lys426, but no binding occurred. At t = 35.25 ns, O1 and O2 formed hydrogen bonds with Lys419, and O6–O8 formed three hydrogen bonds with Lys426 (Figure 3D). At t = 36.35 ns, only O3 of PEG10A/HETC interacted with LIMP-2 through a Lys426 (Figure 3E). At t = 44.85, PEG10A/HETC

https://doi.org/10.1021/acsomega.2c00667
ACS Omega 2022, 7, 15728–15738

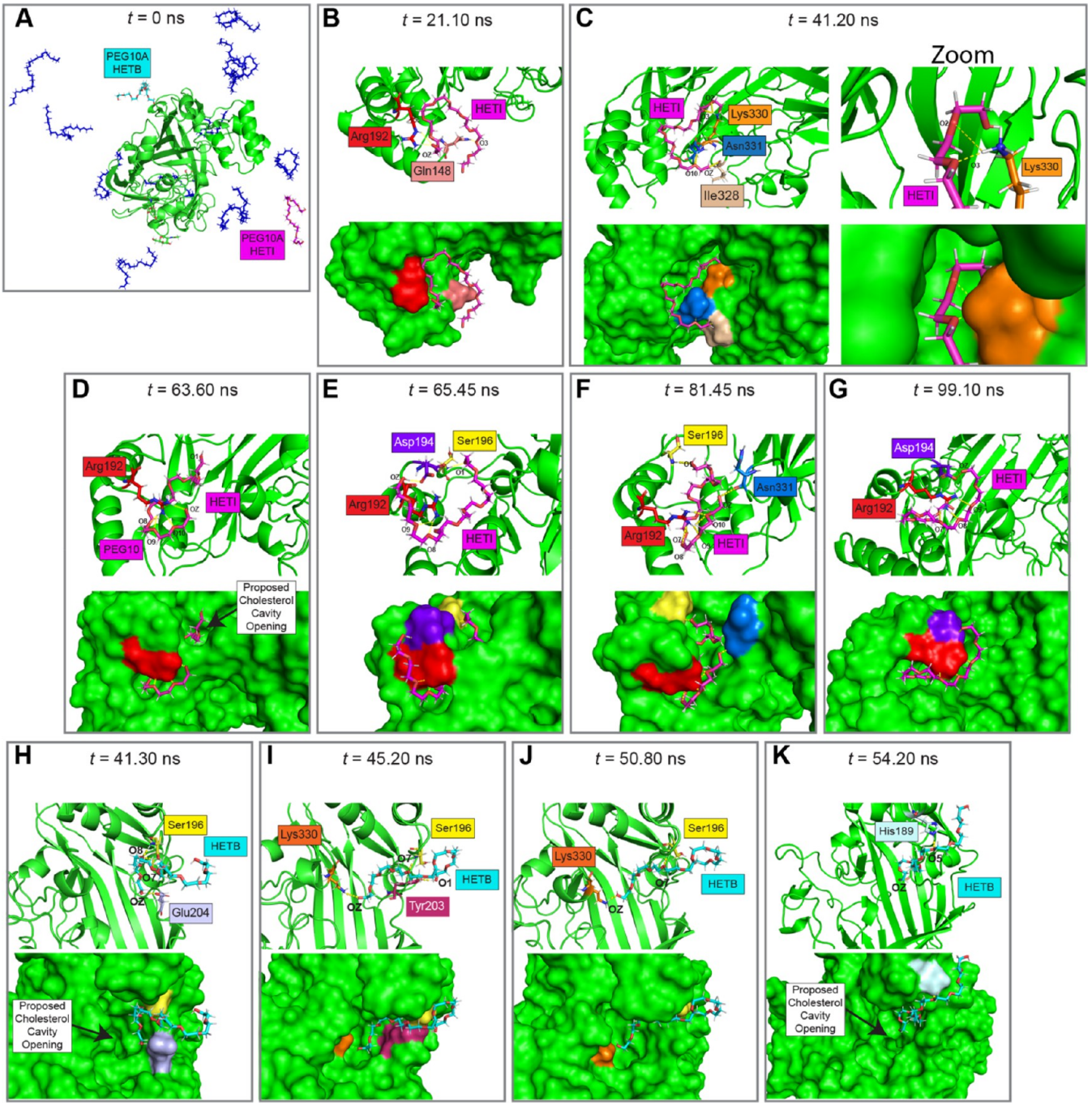

Figure 4. PEG10A/HETI and PEG10A/HETB penetrate LIMP-2. (A) Starting configuration of the simulation where LIMP-2 was surrounded by 13 randomly positioned PEG molecules having 10 monomers each (PEG10). This is the same conformation as in Figure 3A. PEG10A/HETI (magenta) and PEG10A/HETB (cyan) are the focus of this figure. Water and KCl were removed from this image. (B–G) Cartoon and matching space-filled images of PEG10A/HETI interacting with LIMP-2 residues at the indicated time points. (H–K) Cartoon and matching space-filled images of PEG10A/HETB interacting with LIMP-2 residues at the indicated time points.

formed an icosagon-like conformation around Lys426 as guided by five hydrogen bonds between Lys426 and O3–O7 and one hydrogen bond between Ser423 and O1 (Figure 3F). At t = 45.30 ns, the icosagon began to unravel where only hydrogen bonds between O4-Lys426 and O5-Lys426 persisted from the t = 44.85 ns conformation (Figure 3G). At this time, PEG10A/HETC O1 was hydrogen-bonded to Lys419. At t = 46.15 ns, O1–O4 formed four hydrogen bonds with Lys426, causing PEG10A/HETC to wrap around this residue again (Figure 3H). At t = 46.85 ns, O1–O4 were still hydrogen-bonded to Lys426 and O1 was hydrogen-bonded to Ser423 (Figure 3I). At t = 47.55 ns, PEG10A/HETC was normal to the LIMP-2 surface with a large end-to-end distance of 27.4 Å. At this time, O1–O3 were still hydrogen-bonded to Lys426. At t = 47.85 ns, PEG10A/HETC was completely detached from LIMP-2.

The PEG10A/HETI and PEG10A/HETB chains also interacted strongly with LIMP-2 over 110 ns of simulation time (Figure 4A). PEG10A/HETI had a more sustained interaction with LIMP-2 than PEG10A/HETB and is

https://doi.org/10.1021/acsomega.2c00667
ACS Omega 2022, 7, 15728–15738

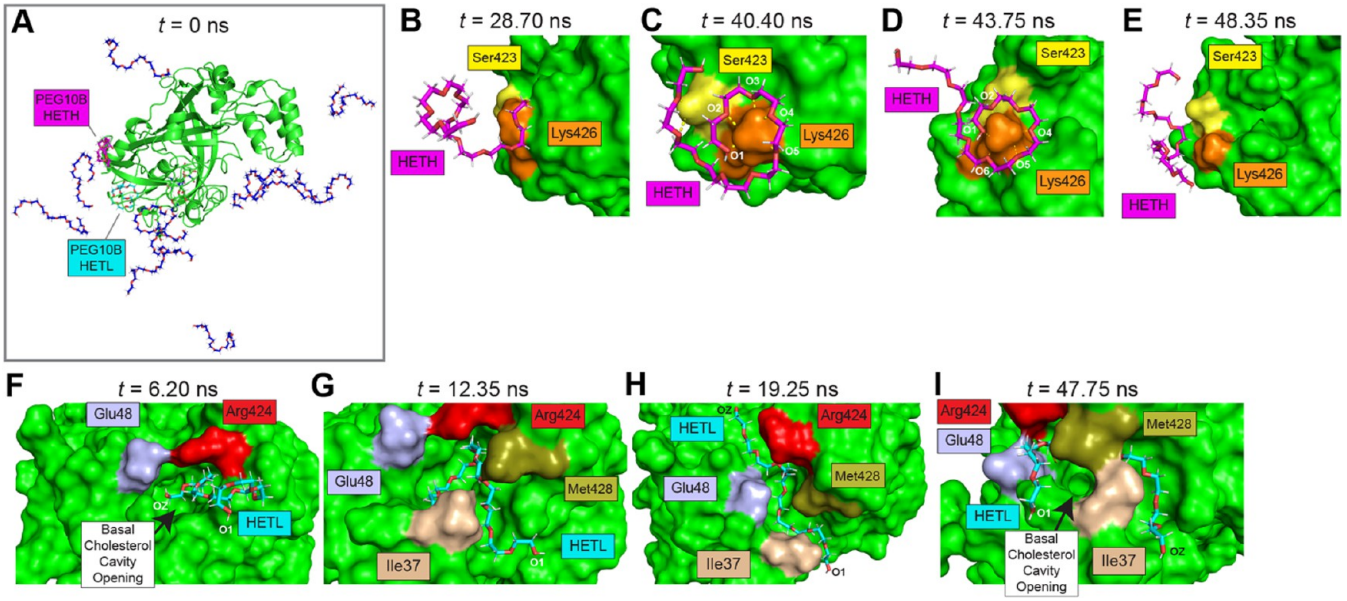

Figure 5. Details of a second PEG10 simulation (PEG10B). (A) Starting configuration of a simulation where LIMP-2 was surrounded by 13 randomly positioned PEG molecules having 10 monomers each (PEG10). PEG10B/HETH (magenta) and PEG10B/HETL (cyan) are the focus of this figure. (B–E) Space-filled images of PEG10B/HETH interacting with LIMP-2 residues at the indicated time points. (F–I) Space-filled images of PEG10B/HETL interacting with LIMP-2 residues at the indicated time points.

discussed first. At t = 21.10 ns, OZ of PEG10A/HETI formed two hydrogen bonds with Arg192, and O3 formed a hydrogen bond with Gln148 (Figure 4B; Movie S5). At t = 41.20 ns, O2 and O3 formed hydrogen bonds with Lys330, O10 formed a hydrogen bond with Asn331, and OZ formed a hydrogen bond with Ile328 (Figure 4C, upper panel). These interactions allowed PEG10A/HETI to enter the cavity by Lys330 and Asn331 (Figure 4C, lower panel). At t = 63.60 ns, O8, O9, O10, and OZ all formed hydrogen bonds with Arg192 (Figure 4D, upper panel). This region of LIMP-2 closed around PEG10A/HETI so that it could not unbind from the protein (Figure 4D, lower panel). At t = 65.45, O1 formed a hydrogen bond with Ser196, O8 and O9 formed hydrogen bonds with Arg192, and OZ formed a hydrogen bond with Asp194 (Figure 4E, upper panel). These residues formed a significant arch or clamp over PEG10A/HETI (Figure 4E, lower panel). At t = 81.45 ns, OZ formed a hydrogen bond with Asn331; O10 formed two hydrogen bonds with Arg192; O7, O8, and O9 formed a hydrogen bond with Arg192; O1 formed a hydrogen bond with Ser196 (Figure 4F, upper panel). At this time, the clamp on PEG10A/HETI begins to open (Figure 4F, lower panel). At t = 99.10 ns, O7, O8, and O9 formed hydrogen bonds with Arg192 and OZ made a hydrogen bond with Asp194 (Figure 4G, upper panel). Here, the OZ of PEG10A/HETI is penetrating LIMP-2 but the rest of HETI is outside the clamp (Figure 4G, lower panel).

In the PEG10A simulation, PEG10A/HETB approached the traditional LIMP-2 cholesterol tunnel opening as defined in ref 4. at $t \sim$ 40 ns (Movie S6). At t = 41.30 ns, O7 formed two hydrogen bonds with Ser196 and Glu204. At the same time, O8 formed two hydrogen bonds with Ser196 (Figure 4H, upper panel). This allowed OZ of PEG10A/HETB to get close to the tunnel opening (Figure 4H, lower panel). At t = 45.20 ns, O1, O7, and OZ formed hydrogen bonds with Tyr330, Ser196, and Lys330 (Figure 4I, upper panel). The hydrogen bond between OZ and Lys330 allowed PEG10/HETB to enter further into the cholesterol cavity (Figure 4I, lower panel). At t = 50.80 ns, OZ was hydrogen bound to Lys330 and O7 was hydrogen bound to Ser196 (Figure 4J, upper panel). The position of OZ was stable from t = 45.20 ns to t = 50.80 ns (Figure 4J, lower panel). At t = 54.20 ns, OZ formed a hydrogen bond with the oxygen on the LIMP-2 backbone between Leu201 and Phe202 and O5 formed a hydrogen bond with His189 (Figure 4K, upper panel). PEG10/HETB dissociated from LIMP-2 at $t \sim$ 60 ns. Thus, PEG10A/HETB stayed bound to the region surrounding the cholesterol tunnel opening for ~20 ns. Note that this interaction is short-lived compared to the PEG10A/HETI interaction.

We ran an additional PEG10 simulation for t = 75 ns, which we called "PEG10B". The goal was to determine the reproducibility of the phenomena observed in the PEG10A simulation. The PEG10 molecules in this simulation are referred to as PEG10B/HET#, where # represents the letter of that heteroatom in the Supporting Information PDB file (LIMP2-PEG10B.pdb). The positions of the PEG10 molecules in the PEG10B are significantly different from the PEG10A system after equilibration (at t = 0 ns) (Figure 5A vs Figures 3A and 4A). The 75 ns movie showing all PEG10B/HET# molecules is presented as Movie S7. PEG10B/HETH wrapped around Lys426 and interacted with Ser423 in an almost identical manner to that of PEG10A/HETC (Figure 5B–E vs Figure 3F; Movie S8). This shows that PEG10 can interact strongly with surface exposed lysine residues. However, in the PEG10A and PEG10B simulations PEG10A/HETC and PEG10B/HETH both unbound from Lys426 and LIMP-2 over the time course of the simulations. In the PEG10B simulation, HETL interacted with the LIMP-2 region that is the proposed base of the cholesterol transport tunnel (Figure 5F–I; Movie S9). This opening is postulated to allow cholesterol to enter the cell through the endolysosome.[4] HETL folded into this region, which is surrounded by four residues: Ile37, Glu48, Arg424, and Met428. The residue pairs Glu48-Arg424 and Il337-Met428 formed gates that clamped

https://doi.org/10.1021/acsomega.2c00667
ACS Omega 2022, 7, 15728–15738

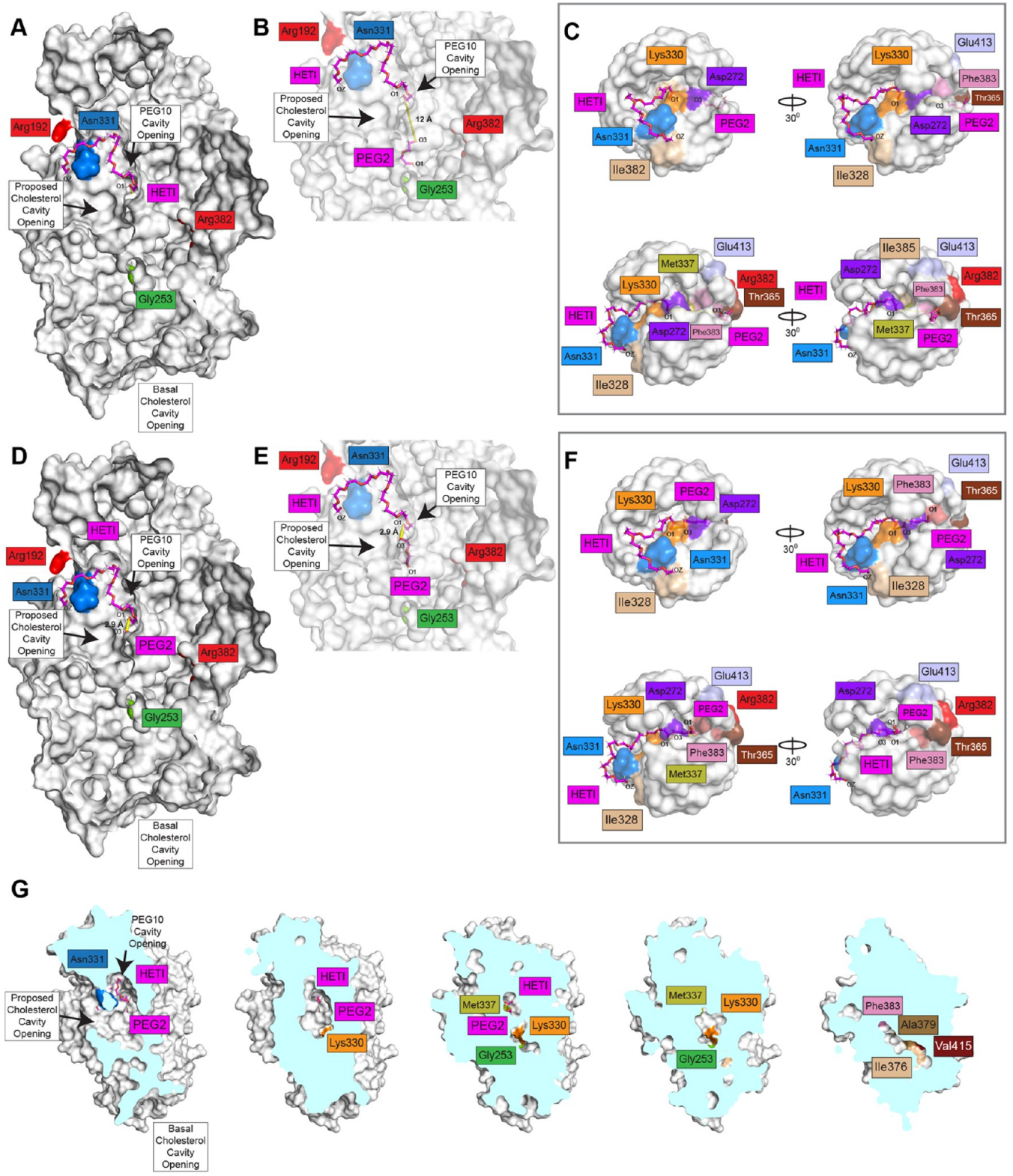

Figure 6. PEG10A/HETI enters the cavity above the proposed cholesterol transport tunnel and comes within 3 Å of PEG2 via this route. (A) Spaced-filled image of the structure of LIMP-2 at t = 41.20 ns (Figure 4C). The cavity that cholesterol is postulated to transport through and the cavity that PEG10 entered are indicated. PEG2 at its position in the equilibrated structure is not visible from the surface. (B) Zoomed in image of (A) where the LIMP-2 surface is transparent to illustrate the location of the tip of PEG10A/HETI and PEG2. O1 of PEG10A/HETI is 12 Å away from O3 of PEG2 in this analysis. (C) Four space-filled images of the structure of LIMP-2 at t = 41.20 ns where only atoms within 15 Å of O1 of PEG10A/HETI are included. Each successive image is rotated 30 degrees in the y-direction. The positions of Met337 and Phe383 sterically hinder the path between PEG10/HETI and PEG2. (D−F) Analogues of (A−C), but the position of PEG2 is obtained from its location at the end our of 50 ns simulation (Figure 2P) instead of its location at the end of the equilibration of 4F7B.pdb. In this analysis, Phe383 flips and allows PEG10A/HETI and PEG2 to come within ∼3 Å of each other. (G) Successive clipping images of LIMP-2 shown in (D). The pockets that are furthest away from the front surface are in the far-right image.

https://doi.org/10.1021/acsomega.2c00667
ACS Omega 2022, 7, 15728−15738

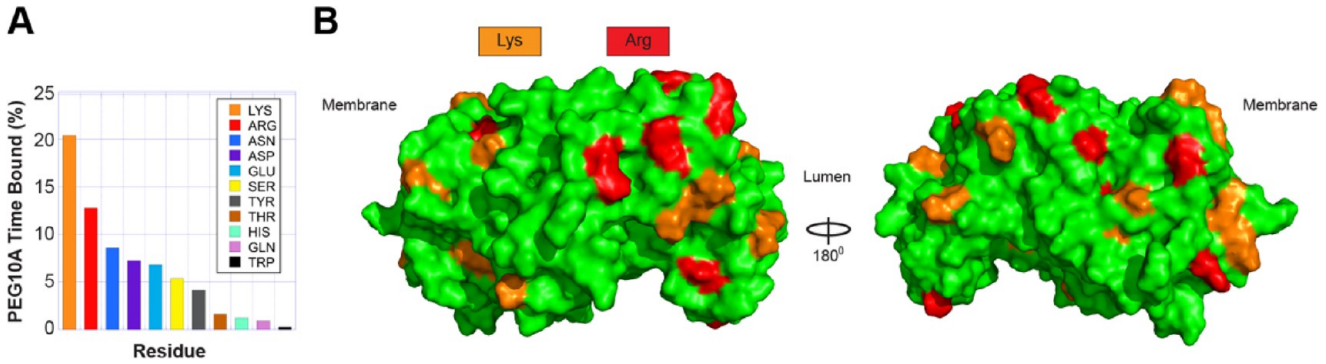

Figure 7. PEG10 interacts most frequently with the lysine and arginine residues of LIMP-2. (A) Plot of the percent time that PEG10 bound the indicated residues in the simulations where 13 PEG10 molecules surrounded LIMP-2. (B) Space-filled models of LIMP-2 where arginine (red) and lysine (orange) are highlighted.

HETL and sustain its close proximity to the tunnel's basal cavity.

PEG10 molecules can be divided into three groups: those that had almost no interactions with LIMP-2, those that had transient interactions with LIMP-2, and those that had persistent interactions with LIMP-2. PEG10 molecules in the first category barely touch the surface of LIMP-2. Those include all HET# molecules not mentioned in the text. The conformations assumed by these PEG10 molecules are what would be expected from a flexible polymer: entropy dominates. PEG10 molecules in the second category into which PEG10A/HETC, PEG10A/HETB, and PEG10B/HETH fall formed multiple hydrogen bonds with LIMP-2, but the strength of the bonds was not enough to overcome the dynamics of PEG10. Both PEG10A/HETI and PEG10B/HETL fall into the third category. They stayed bound to LIMP-2 from t = 21.10 to 110 ns and from t = 0 to 75 ns, respectively. The extended interaction times are sustained by residue gates or clamps. HETI in the PEG10A simulation was held in place by the gate formed by Arg192 which closed around HETI and blocked its unbinding (Figure 4D,E and Movie S5). On the other hand, HETB in the PEG10A simulation entered the proposed cholesterol tunnel opening but did not have enough persistent bonds or steric support, such as a gate or clamp, to allow further penetration into the cavity (Movie S6). It is difficult to see how PEG could enter the proposed cholesterol cavity directly through this path. It most likely enters through the top where it can be stabilized by the aforementioned gates or clamps. Like the dynamics of HETI in the PEG10A simulation, the gates formed by Glu48-Arg424 and Ile37-Met428 closed behind HETL in the PEG10B simulation and kept HETL associated with the basal entrance to the cholesterol tunnel (Movie S9). We postulate that dynamic, knob-like residue domains are necessary for PEG−protein binding.

To explore the interaction of HETI with LIMP-2 in the PEG10A simulation in more detail, we overlaid the equilibrated LIMP-2−PEG2 structure with the LIMP-2−PEG10 structure at t = 41.20 ns as shown in Figure 4C (Figure 6A). PEG10A/HETI appears to enter a cavity that is just above the proposed cholesterol cavity, below Asn331. PEG10A/HETB entered the proposed cholesterol cavity itself but had a weaker overall interaction with LIMP-2 in that region based on the reduced amount of time that it was bound. As stated above, we postulate that this is due to flexible residue clamping around PEG10. The distance between O1 of PEG10A/HETI and the closest oxygen of PEG2 (O3) is 12 Å (Figure 6B). We wished to determine if the tunnels occupied by PEG2 and PEG10 connected. To do so visually, we reserved all atoms within 15 Å of O1 of PEG10A/HETI. This model is a sphere that contains PEG10A/HETI, PEG2, and the surrounding residues, without the visual encumbrance of the rest of LIMP-2. From the images, PEG2 and PEG10A/HETI would have a difficult time meeting, i.e., going through the same cavity - given the steric hindrances of Asp272, Met337, and Phe383 (Figure 6C). However, PEG2 moved toward PEG10A/HETI at t = 52 ns (Figure 2Q). We performed the same overlay, but instead of using the equilibrated LIMP-2 − PEG2 model, we used the 60 ns LIMP-2 − PEG2 conformation. In this model, PEG2 was within 2.9 Å of PEG10A/HETI (Figure 6D,E). PEG2 navigated past Phe383 and is in the same cavity as PEG10A/HETI (Figure 6F). That PEG10A/HETI and PEG2 share the same cavity can also be seen when LIMP-2 is clipped from the near plane (Figure 6G). As the clipping is increased from left to right in Figure 6G, the cavity from the point of PEG10A/HETI insertion to PEG2 to the residues that are postulated to be responsible for cholesterol transport (Ala379, Val415) appears to be a continuous tunnel (Figure 6G).

PEG10 had the highest affinity for lysine and arginine (Figure 7A). The NH_3^+ group of lysine can form three hydrogen bonds. Also, its slightly hydrophobic stem may increase interactions with the C−C motif of PEG. The arginine side chain is the most basic of the amino acids (pK 12.5). Its positive charge is stabilized by resonance. It is unique among amino acids for having five hydrogen-bonding donor atoms (NE (1), NH1 (2), and NH2 (2)). Since PEG can have numerous oxygen donor atoms along its backbone, arginine and PEG can form tight associations, as observed in our simulation. LIMP-2 has ∼25 surface exposed lysine and arginine residues (Figure 7B). Their hydrogen-bonding capabilities and exposure make them ideal for binding PEG.

Changing the length of PEG in either experiments or simulations will result in both increased PEG entropy and increased number of oxygens on the PEG backbone that can interact with hydrogen bonding residues on the surface of the protein. It is unclear what the trade-off will be. The results here lead to the postulate that the ability of a long PEG molecule to bind a protein will be a function of the number of exposed arginine and lysine residues but most importantly, the close proximity of gates to these two residues.

https://doi.org/10.1021/acsomega.2c00667
ACS Omega 2022, 7, 15728−15738

4. CONCLUSIONS

The simulations show that PEG can bind and enter protein cavities over short time scales if surface-exposed lysines and arginines are available for hydrogen binding, and protruding, dynamic residue groups are available to clamp down on PEG. The only other atomistic-scale structural study of single PEG and protein that we are aware of, besides the LIMP-2 work, is the structure of PEG and its antibody.[6] In that work, PEG wraps around a surface-exposed tryptophan (Trp96) of anti-PEG Fab.[6] LIMP-2 has three surface-exposed tryptophans: Trp146, Trp239, and Trp261. Of the 11 residues that can form hydrogen bonds with PEG, tryptophan had the lowest interaction with the 13 PEG molecules that surrounded LIMP-2 (Figure 7A). Thus, PEG does not appear to interact strongly with tryptophan on the surface of LIMP-2 over the time course of our NAMD simulations.

PEG's ability to enter the proposed cholesterol binding pocket of LIMP-2 is of great relevance to PEG-based nanomedicines. It has been shown that PEG nanoparticles compete with high-density lipoprotein (HDL) for SR-BI.[5] Here, we provide a potential mechanism for this competitive binding using the homologous LIMP-2 protein as a model CD36 family member. The pharmacokinetics, pharmacodynamics, toxicity, and efficacy of PEG-based nanomedicines may be greatly affected by lipoprotein and cholesterol levels.

ASSOCIATED CONTENT

Supporting Information

The Supporting Information is available free of charge at https://pubs.acs.org/doi/10.1021/acsomega.2c00667.

LIMP-2 apo dynamics (MPG)
LIMP-2 PEG2 dynamics (MPG)
LIMP-2 PEG10A dynamics (MPG)
LIMP-2 PEG10A/HETC dynamics (MPG)
LIMP-2 PEG10A/HETI dynamics (MPG)
LIMP-2 PEG10A/HETB dynamics (MPG)
LIMP-2 PEG10B dynamics (MPG)
LIMP-2 PEG10B/HETH dynamics (MPG)
LIMP-2 PEG10B/HETL dynamics (MPG)
Characterization data for LIMP-2 apo (PDB)
Characterization data for LIMP-2 PEG2 (PDB)
Characterization data for LIMP-2 PEG10A (PDB)
Characterization data for LIMP-2 PEG10B (PDB)

AUTHOR INFORMATION

Corresponding Author

Paul Dalhaimer − *Department of Chemical and Biomolecular Engineering and Department of Biochemistry, Cellular, and Molecular Biology, University of Tennessee, Knoxville, Tennessee 37996, United States;* orcid.org/0000-0003-2929-3372; Email: pdalhaim@utk.edu

Author

Kate R. Blankenship − *Department of Chemical and Biomolecular Engineering, University of Tennessee, Knoxville, Tennessee 37996, United States*

Complete contact information is available at: https://pubs.acs.org/10.1021/acsomega.2c00667

Notes

The authors declare no competing financial interest.

ACKNOWLEDGMENTS

The authors thank Xianfeng Ma for assistance setting up and running the simulations on the University of Tennessee's Isaac Cluster.

ABBREVIATIONS

PEG, polyethylene glycol; LIMP-2, lysosomal integral membrane protein-2; CD36, cluster of differentiation 36; SR-BI, scavenger receptor class B I; HDL, high-density lipoprotein; SARS-CoV-2, severe acute respiratory syndrome coronavirus 2; PEG2, poly ethylene-glycol with two monomers; PEG10, poly ethylene-glycol with ten monomers; PEG10A, first simulation with 13 PEG10 molecules surrounding LIMP-2; PEG10B, second simulation with 13 PEG10 molecules surrounding LIMP-2; HET, heteroatom in the protein data bank lexicon

REFERENCES

(1) Jokerst, J. V.; Lobovkina, T.; Zare, R. N.; Gambhir, S. S. Nanoparticle PEGylation for imaging and therapy. *Nanomedicine* **2011**, *6* (4), 715−728.

(2) Suk, J. S.; Xu, S.; Kim, N.; Hanes, J.; Ensign, L. M. PEGylation as a strategy for improving nanoparticle-based drug and gene delivery. *Adv. Drug Delivery Rev.* **2016**, *99* (Pt A), 28−51.

(3) Kristensen, K.; Engel, T. B.; Stensballe, A.; Simonsen, J. B.; Andresen, T. L. The hard protein corona of stealth liposomes is sparce. *J. Controlled Release* **2019**, *307*, 1−15.

(4) Neculai, D.; Schwake, M.; Ravichandran, M.; Zunke, F.; Collins, R. F.; Peters, J.; Neculai, M.; Plumb, J.; Loppnau, P.; Pizarro, J. C.; Seitova, A.; Trimble, W. S.; Saftig, P.; Grinstein, S.; Dhe-Paganon, S. Structure of LIMP-2 provides functional insights with implications for SR-BI and CD36. *Nature* **2013**, *504* (7478), 172−176.

(5) Raith, M.; Kauffman, S. J.; Asoudeh, M.; Buczek, J. A.; Kang, N.-G.; Mays, J. W.; Dalhaimer, P. Elongated PEG-based nanoparticles bind the high-density lipoprotein (HDL) receptor scavenger receptor class B I (SR-BI). *J. Controlled Release* **2021**, *337* (2021), 448−457.

(6) Huckaby, J. T.; Jacobs, T. M.; Li, Z.; Perna, R. J.; Wang, A.; Nicely, N.; Lai, S. K. Structure of an anti-PEG antibody reveals an open ring that captures highly flexible PEG polymers. *Communications Chemistry* **2020**, 3, 124.

(7) Jo, S.; Kim, T.; Iyer, V. G.; Im, W. CHARMM-GUI: A web-based graphical user interface for CHARMM. *J. Comput. Chem.* **2008**, *29* (11), 1859−1965.

(8) Brooks, B. R.; Brooks, C. L., III; MacKerell, A. D., Jr.; Nilsson, L.; Petrella, R. J.; Roux, B.; Won, Y.; Archontis, G.; Bartels, C.; Boresch, S.; Caflisch, A.; Caves, L.; Cui, Q.; Dinner, A. R.; Feig, M.; Fischer, S.; Gao, J.; Hodoscek, M.; Im, W.; Kuczera, K.; Lazaridis, T.; Ma, J.; Ovchinnikov, V.; Paci, E.; Pastor, R. W.; Post, C. B.; Pu, J. Z.; Schaefer, M.; Tidor, B.; Venable, R. M.; Woodcock, H. L.; Wu, X.; Yang, W.; York, D. M.; Karplus, M. CHARMM: The biomolecular simulation platform. *J. Comput. Chem.* **2009**, *30* (10), 1545−1614.

(9) Lee, J.; Cheng, X.; Swails, J. M.; Yeom, M. S.; Eastman, P. K.; Lemkul, J. A.; Wei, S.; Buckner, J.; Jeong, J. C.; Qi, Y.; Jo, S.; Pande, V. S.; Case, D. A.; Brooks, C. L., III; Mackerell, A. D., Jr.; Klauda, J. B.; Im, W. CHARMM-GUI input generator for NAMD, GROMACS, AMBER, OpenMM, and CHARM/OpenMM simulation using the CHARMM36 additive force field. *J. Chem. Theory Comput.* **2016**, *12* (1), 405−413.

(10) Jo, S.; Song, K. C.; Desaire, H.; MacKerell, A. D., Jr.; Im, W. Glycan reader: automated sugar identification and simulation for carbohydrates and glycoproteins. *J. Comput. Chem.* **2011**, *32* (14), 3135−3141.

(11) Park, S.-J.; Lee, J.; Patel, D. S.; Ma, H.; Lee, H. S.; Jo, S.; Im, W. Glycan reader is improved to recognize most sugar types and chemical modifications in the protein data bank. *Bioinformatics* **2017**, *33* (19), 3051−3057.

(12) Park, S.-J.; Lee, J.; Qi, Y.; Kern, N. R.; Lee, H. S.; Jo, S.; Joung, I.; Joo, K.; Lee, J.; Im, W. CHARMM-GUI glycan modeler for modeling and simulation of carbohydrates and glycoconjugates. *Glycobiology* **2019**, *29* (4), 320−331.
(13) Thier, S. O. Potassium physiology. *Am. J. Med.* **1986**, *80* (4A), 3−7.
(14) Choi, Y. K.; Park, S.-J.; Park, S.; Kim, S.; Kern, N. R.; Lee, J.; Im, W. CHARMM-GUI polymer builder for modeling and simulation of synthetic polymers. *J. Chem. Theory Comput.* **2021**, *17* (4), 2431−2443.
(15) Phillips, J. C.; Hardy, D. J.; Maia, J. D. C.; Stone, J. E.; Ribeiro, J. V.; Bernardi, R. C.; Buch, R.; Fiorin, G.; Henin, J.; Jiang, W.; McGreevy, R.; Melo, M. C. R.; Radak, B. K.; Skeel, R. D.; Singharoy, A.; Wang, Y.; Roux, B.; Aksimentiev, A.; Luthey-Schulten, Z.; Kale, L. V.; Schulten, K.; Chipot, C.; Tajkhorshid, E. Scalable molecular dynamics on CPU and GPU architectures with NAMD. *J. Chem. Phys.* **2020**, *153* (4), 044130.
(16) Humphrey, W.; Dalke, A.; Schulten, K. VMD: visual molecular dynamics. *J. Mol. Graphics* **1996**, *14* (1), 33−38.
(17) Canton, J.; Neculai, D.; Grinstein, S. Scavenger receptors in homeostasis and immunity. *Nat. Rev. Immunol.* **2013**, *13* (9), 621−634.
(18) Heybrock, S.; Kanerva, K.; Meng, Y.; Ing, C.; Liang, A.; Xiong, Z.-J.; Weng, X.; Ah Kim, Y.; Collins, R.; Trimble, W.; Pomes, R.; Prive, G. G.; Annaert, W.; Schwake, M.; Heeren, J.; Lullmann-Rauch, R.; Grinstein, S.; Ikonen, E.; Saftig, P.; Neculai, D. Lysosomal integral membrane protein-2 (LIMP-2/SCARB2) is involved in lysosomal cholesterol export. *Nat. Commun.* **2019**, *10*, 3521.
(19) Lee, J.; Hitzenberger, M.; Rieger, M.; Kern, N. R.; Zacharias, M.; Im, W. CHARMM-GUI supports the Amber force fields. *J. Chem. Phys.* **2020**, *153* (3), 035103.

https://doi.org/10.1021/acsomega.2c00667
ACS Omega 2022, 7, 15728−15738